analytical chemistry

pubs.acs.org/ac Article

AFM-Based High-Throughput Nanomechanical Screening of Single Extracellular Vesicles

Andrea Ridolfi, Marco Brucale,* Costanza Montis, Lucrezia Caselli, Lucia Paolini, Anne Borup, Anders T. Boysen, Francesca Loria, Martijn J. C. van Herwijnen, Marije Kleinjan, Peter Nejsum, Natasa Zarovni, Marca H. M. Wauben, Debora Berti, Paolo Bergese, and Francesco Valle*

Cite This: *Anal. Chem.* 2020, 92, 10274−10282 Read Online

ACCESS | Metrics & More | Article Recommendations | Supporting Information

ABSTRACT: The mechanical properties of extracellular vesicles (EVs) are known to influence their biological function, in terms of, e.g., cellular adhesion, endo/exocytosis, cellular uptake, and mechanosensing. EVs have a characteristic nanomechanical response which can be probed via force spectroscopy (FS) and exploited to single them out from nonvesicular contaminants or to discriminate between subtypes. However, measuring the nanomechanical characteristics of individual EVs via FS is a labor-intensive and time-consuming task, usually limiting this approach to specialists. Herein, we describe a simple atomic force microscopy based experimental procedure for the simultaneous nanomechanical and morphological analysis of several hundred individual nanosized EVs within the hour time scale, using basic AFM equipment and skills and only needing freely available software for data analysis. This procedure yields a "nanomechanical snapshot" of an EV sample which can be used to discriminate between subpopulations of vesicular and nonvesicular objects in the same sample and between populations of vesicles with similar sizes but different mechanical characteristics. We demonstrate the applicability of the proposed approach to EVs obtained from three very different sources (human colorectal carcinoma cell culture, raw bovine milk, and *Ascaris suum* nematode excretions), recovering size and stiffness distributions of individual vesicles in a sample. EV stiffness values measured with our high-throughput method are in very good quantitative accord with values obtained by FS techniques which measure EVs one at a time. We show how our procedure can detect EV samples contamination by nonvesicular aggregates and how it can quickly attest the presence of EVs even in samples for which no established assays and/or commercial kits are available (e.g., *Ascaris* EVs), thus making it a valuable tool for the rapid assessment of EV samples during the development of isolation/enrichment protocols by EV researchers. As a side observation, we show that all measured EVs have a strikingly similar stiffness, further reinforcing the hypothesis that their mechanical characteristics could have a functional role.

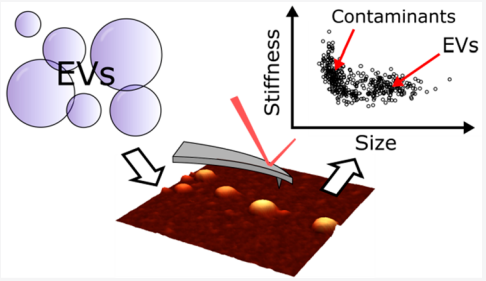

Extracellular vesicles (EVs) are cell-released, submicrometer membranous particles involved in numerous physiological and pathological functions.[1,2] Due to their almost ubiquitous relevance, they are focalizing the interest of a rapidly growing, highly multidisciplinary research community including oncologists, neurologists, bioengineers, parasitologists, cell biologists, food scientists, and biophysicists.[3−9] Because of the diverse biogenesis/release mechanisms of EVs and their enormous heterogeneity, the EV community is making a continuous effort to reach a consensus regarding several fundamental issues, including EV nomenclature.[10]

The vast majority of experimental research on EVs of any type starts with their isolation, purification, and enrichment—which are nontrivial endeavors, often needing sample-specific protocol optimization to limit contamination by nonvesicular material or excessive EV size polydispersion.[11−14] Furthermore, the analysis of EV samples is made difficult by a general scarcity of established tools for characterizing EVs with highly varied size, origin, function, membrane lipid/protein composition, and cargo content.[10,15] Some of the most powerful EV characterization techniques (e.g., cryo-EM) are highly demanding in terms of costs, time, and expertise. Hence, there is a need to develop methods for rapid, label-free assessment of EV samples, which are able to discern between vesicular and nonvesicular particles in the submicrometer range and are applicable to EVs isolated from highly diverse sources. In this context, single-vesicle measurements seem especially promising.[16]

One relatively constant feature of EVs isolated from different sources is their mechanical behavior, which is known to be influential on cellular adhesion, endo/exocytosis, cellular

Received: December 18, 2019
Accepted: July 7, 2020
Published: July 7, 2020

https://dx.doi.org/10.1021/acs.analchem.9b05716
Anal. Chem. 2020, 92, 10274−10282

uptake, and mechanosensing.[17] EVs have been shown to give a characteristic mechanical response to an applied load: a highly linear force/distance elastic deformation regime, which is also typical of synthetic liposomes but is otherwise very uncommon in nonvesicular objects.[18−21] This characteristic behavior can be recognized by probing the mechanical response of individual vesicles deposited on a substrate via atomic force microscope (AFM)-based force spectroscopy (FS).[22] The linear deformation regime slope reflects the vesicle's overall stiffness (k_S), i.e., its resistance to deformation, and can be quantitatively measured via AFM-FS nanoindentation experiments. Specific types of EV were observed to have characteristic k_S values, which can vary in the presence of pathological processes.[21,23] Due to this, it seems reasonable to consider mechanical response in general, and k_S in particular, as the basis for a method capable of discriminating EVs from contaminants or even between different types of EVs.

The observed linear mechanical response of vesicles is best rationalized by the Canham−Helfrich (CH) model,[24,25] in which the overall stiffness k_S is the sum of two contributing factors: membrane rigidity, quantified by its bending modulus (κ), and luminal pressurization (Π). Wuite and co-workers recently demonstrated that AFM-FS can be employed to separately determine the κ and Π values of individual liposomes,[26] that the same approach is applicable to EVs,[21] and that it can detect quantitative mechanical behavior variations linked to biological function.[17] This elegant and powerful AFM-FS approach is however quite labor-intensive, requiring the experimental determination of k_S, tether elongation force (F_T), and curvature radius (RC) for each individual vesicle. In particular, obtaining clear F_T readings involves the establishment of a single mechanical link between the vesicle's membrane and the AFM probe and can be problematic on EVs with abundant membrane proteins and/or lipopolysaccharides content. Finally, it is necessary to pool the readings of at least several tens of individual vesicles to obtain a reasonably clear picture of an EVs population's overall mechanical characteristics. Combined together, these considerations imply that the FS-based strategy mentioned above is in our opinion the best currently available method to obtain a quantitative mechanical characterization of individual vesicles but is also poorly suited to a quick, routine screening of unknown EV samples mainly aimed at achieving a broad picture of their size distribution and purity.

We herein propose a method for the rapid nanomechanical assessment of EV populations based on simple AFM imaging performed in liquid and successive morphometric analysis easily performed with freely available software. Following the procedure detailed in the following sections, it is possible to define the size and mechanical characteristics of a few hundred individual vesicles in the hour time scale in ideal experimental conditions. Although the mechanical readout provided by our procedure is semiquantitative, it is able to discriminate between subpopulations of vesicular and nonvesicular objects deposited on the same substrate and between populations of vesicles with similar sizes but different mechanical characteristics. Moreover, we show a calibration procedure that can be used to estimate the k_S of EVs without performing FS experiments.

As a proof of concept, we demonstrate the applicability of our method to EV samples isolated from three purposedly very different natural sources: human colorectal carcinoma (HCT116) cell culture, raw bovine milk, and the excretory/secretory products of the parasitic nematode *Ascaris suum*. Being so dissimilar, the selected sources must be subjected to very different isolation/enrichment procedures to obtain EV samples. Nevertheless, our method is able to assess the presence of vesicles and/or contaminants in aliquots of each sample and to yield a distribution of size and nanomechanical characteristics of hundreds of individual EVs within several hours. It is worthwhile to add that we were able to quickly verify the presence of vesicles with the "typical" nanomechanical characteristics of EVs in the *Ascaris suum* samples, whose characterization is otherwise still challenging, e.g., due to the current lack of specific protein markers. This suggests that our method could help the iterative optimization of isolation/enrichment protocols of other currently uncharacterized EVs.

EXPERIMENTAL SECTION

Full details about synthetic and natural vesicles preparation, characterization, and surface immobilization are given in the Supporting Information (see below).

We refer the reader to the Supporting Information section also for experimental details on AFM setup, AFM imaging conditions, and AFM force spectroscopy measurements.

Quantitative AFM Morphometry of Vesicles. The mechanical characterization of vesicles via quantitative AFM morphometry was performed as follows. Representative AFM micrographs (typically 5 × 5 μm, 512 × 512 points) were first acquired as described above. Since all the following image analysis steps rely on a correct zero-height baseline assignment, special care was taken to ensure that the image was devoid of image flattening artifacts by masking all positive features appearing on the surface and excluding them from linear background interpolation. In some cases, it was necessary to iterate the masking/subtraction procedure several times to obtain the required background flatness.

Figure S2a exemplifies a correctly processed AFM image of DPPC liposomes: after background subtraction, height profiles measured along the diagonals of the whole image (Figure S2b) are extremely flat, and the average height of empty areas is zero. Moreover, height profiles measured along the X and Y axis for individual vesicles are symmetrical and almost superimposable (Figure S2c), denoting that probe-induced deformation of vesicles along the fast scan axis is marginal.

Putative vesicles are then singled out from the background by marking all pixels exceeding a height threshold (Figure S2a). The employed threshold value was 10 nm in all cases except for DOPC samples, for which we employed a 5 nm threshold (for reasons explained below). Objects touching any edge of the image were automatically excluded from successive analysis. We then manually excluded objects evidently corresponding to clusters of two or more adjoining globular objects or to imaging artifacts such as vesicles that detached themselves from the surface between successive scan lines, resulting in nonglobular shapes with sharp drops along the slow scan axis (Figure S2d). The radius of the largest possible inscribed disc was then calculated for each object (Figure S2d, white circles); those with an inscribed circle radius <10 nm were discarded to exclude spikes and streaks from successive analysis.

Figure S2e shows a representative AFM image of a single putative DPPC vesicle. Our morphometrical analysis starts with the consideration that the shape observed in AFM micrographs is the combination of the vesicle's true shape,

https://dx.doi.org/10.1021/acs.analchem.9b05716
Anal. Chem. 2020, 92, 10274−10282

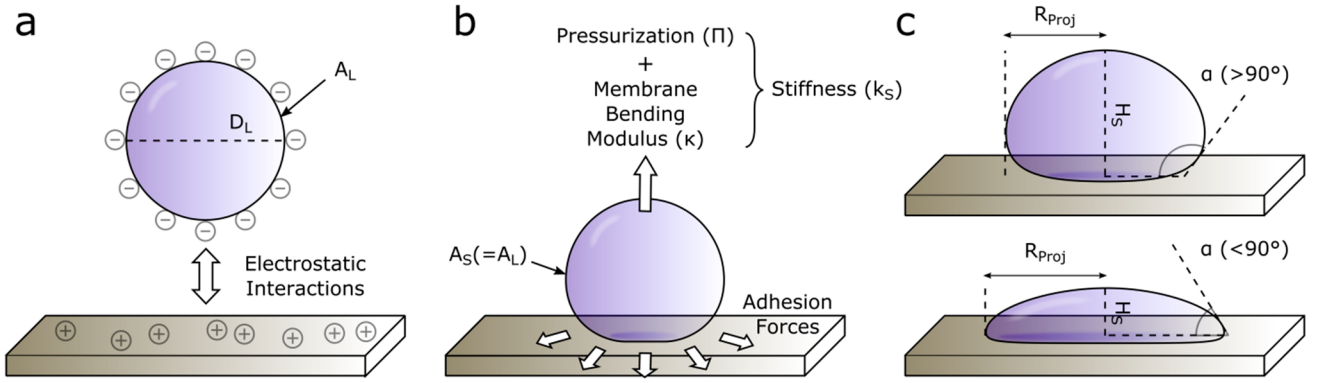

Figure 1. Schematic depiction of the surface adhesion process of a vesicle. (a) In liquid, the vesicle's average shape is a sphere with diameter D_L ("diameter in liquid") and corresponding total membrane area A_L ("area in liquid"). All vesicles utilized in this study have a negative ζ-potential in ultrapure water and are thus electrostatically attracted to substrates coated with poly-L-lysine. (b) When the vesicle first contacts the substrate, adhesive forces tend to maximize surface/membrane contact, causing the deformation of its previously spherical shape into an increasingly oblate spheroid. Membrane stretching is assumed to be negligible throughout the whole process, and thus the total membrane area of the vesicle on the surface (A_S) is equal to A_L (see panel a). The vesicle resists deformation to a degree quantified by its membrane bending modulus κ and internal pressurization Π, which jointly contribute to overall stiffness (k_S). (c) The equilibrium geometry of the adsorbed vesicle is thus a function of its stiffness k_S (see panel b) and can be quantified in terms of height H_S and projected radius R_{Proj}. These two values can be used to calculate the vesicle's contact angle α, which describes the entity of its oblate deformation independently from its size; α will be >90° when $H_S > R_{Proj}$ (top) and <90° in the opposite case (bottom). Comparatively stiffer vesicles will experience smaller deformations and will thus have larger measured α (top) than softer ones (bottom).

probe convolution, feedback artifacts, and the intrinsic AFM limitation of not being able to follow the shape of objects with fractal dimension above 1 along the Z axis.[27] Images can be optimized for minimal feedback artifacts (as discussed above), and their quantitative analysis can take probe convolution into account (see Figure S3). The observed AFM morphology is thus assumed to be a close "pseudo-3D" rendition of the examined object, resulting from the combination of the object's true height values measured along the Z axis and its projection on the XY plane. According to this, a globular object's true maximum surface height H_S and projected surface radius R_{Proj} can be quantitatively measured from its AFM image (Figure S2e): H_S is simply its maximum Z value, while R_{Proj} corresponds to its maximum inscribed disc radius corrected for tip convolution (see Figures S3 and S4).

We then assume that the spheroid shape of a surface-adhered vesicle can be approximated to that of a spherical cap[28] with a height equal to H_S and a projected surface radius equal to R_{Proj} (Figure S2f). The vesicle's projected radius R_{Proj} is used as the best approximation of its curvature radius (R_{Cap}) if $R_{Proj} < H_S$ (Figure S2f, left panel) and of its base radius (A_{Cap}) if $R_{Proj} > H_S$ (Figure S2f, right panel). The corresponding vesicle−surface contact angle (α, see Figure S2f) and total membrane area (A_S, see Figure 1) can be obtained via simple trigonometry calculations (see the Supporting Information). Finally, we estimate the vesicle's size in solution by assuming that even if its shape (originally spherical) was distorted upon interaction with the surface, its membrane underwent negligible stretching,[29] thus allowing us to calculate the diameter of a sphere of area A_L equal to the A_S value recovered from AFM imaging (Figure 1).

RESULTS AND DISCUSSION

Nanomechanical Screening of Vesicles via AFM Imaging. The rationale for our mechanical screening methodology is schematized in Figure 1. In the absence of external perturbations, the average shape of a vesicle in solution is spherical (Figure 1a) and can be geometrically characterized in terms of its diameter (D_L) and total surface area (A_L). Most, if not all, EVs have a negative surface charge[30−32] and can adhere to positively charged surfaces by electrostatic interactions exerting an attractive force between its membrane and the substrate.[28] Upon interaction, adhesion forces deform the initially spherical vesicle into an increasingly oblate shape. This deformation is opposed by both membrane rigidity and luminal pressurization, which jointly contribute to the vesicle's observed stiffness (Figure 1b). The extent to which a surface-adhered vesicle is deformed at equilibrium is thus a function of its stiffness, with higher k_S values resulting in smaller geometrical distortions and softer vesicles assuming more oblate shapes.[33] The vesicle−surface contact angle (α) can be employed as a size-independent quantitative descriptor of the adhered vesicle's deformation (Figure 1c).

With the opportune precautions (see the Supporting Information), simple AFM imaging in liquid can be used to determine the unperturbed equilibrium geometry of EVs deposited on a substrate in terms of their height H_S and surface-projected radius R_{Proj} (Figure 1c). These values can be used to calculate each vesicle's contact angle α and (assuming membrane area conservation during deformation) its original solution diameter D_L.

It is worthwhile to note that the membrane area conservation assumption[26,34] we use is just a useful simplification of the complex interplay of phenomena occurring when a vesicle electrostatically adheres to a surface; an alternative approach reported in the literature is to instead assume volume conservation.[35−38] Although theoretically incompatible, both approaches yielded accurate vesicular size characterization in different AFM-based studies.[17,39] We chose the area conservation assumption on the basis of the fact that in our hands it yielded the best accord between AFM morphometry and other vesicle sizing techniques (see below); most importantly, analyzing our data assuming volume conservation would imply hypothesizing that, upon surface adhesion, vesicles were able to stretch their surface area by very

https://dx.doi.org/10.1021/acs.analchem.9b05716
Anal. Chem. 2020, 92, 10274−10282

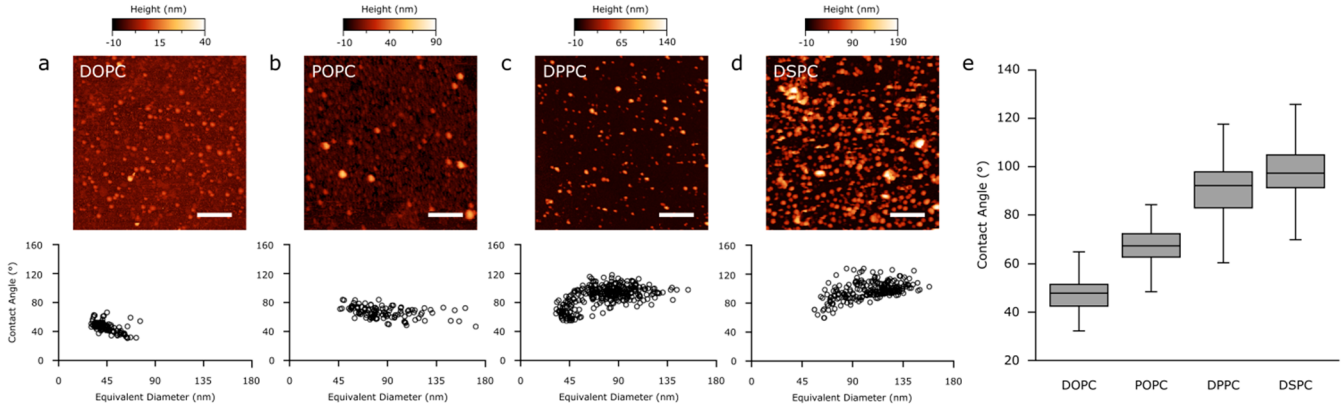

Figure 2. (a–d) Representative AFM images (top) and contact angle vs equivalent diameter scatterplots (bottom) of (a) DOPC, (b) POPC, (c) DPPC, and (d) DSPC liposomes. All scale bars are 1 μm. (e) Box plot comparison of liposome contact angle distributions. Gray boxes extend between the first (bottom edge) and third (top edge) quartile values, with black lines indicating median values. Whiskers correspond to the lowest (bottom) and highest (top) value found within the distribution. *t* tests performed on all pairs of distributions give *p*-values $\leq$0.0001.

large amounts (up to ~250%) without rupturing, which we rejected as unphysical.

It is also important to note that CH theory assumes κ to be an intrinsic property of vesicles formed by the same type of membrane, while k_S is expected to vary with vesicle size.[40] However, we hypothesize that k_S variations observed within populations of vesicles of the same type will be relatively small in the relatively narrow size distribution most relevant to EV research (30–500 nm in diameter). If this is true, populations of compositionally similar vesicles should show a limited dispersion of α values across different vesicle sizes, possibly small enough to resolve their distributions.

Vesicles of the Same Type Have a Characteristic Average Contact Angle Value. To verify the above hypothesis on the simplest possible vesicular objects, we first prepared solutions of synthetic liposomes having a negative ζ-potential (DOPC, POPC, DPPC, and DSPC) in ultrapure water, deposited them on PLL-coated substrates, captured their adhered morphology with in-liquid AFM imaging, and then calculated α and D_L values for several hundreds of individual vesicles. For each type of liposome, we plotted the calculated values of all individual vesicles as points on α versus D_L graphs (Figure 2a–d). The α values of DOPC and POPC vesicles seem to be weakly negatively correlated with their size, while DPPC and DSPC plots suggest the opposite trend. It is interesting to note that in all cases, most of the deviation from a horizontal, flat distribution occurs in smaller (D_L < 50 nm) vesicles, while larger ones seem to converge toward an average α value. Despite these deviations, all the examined liposome types show a relatively narrow global distribution of contact angle values at all observed diameters D_L, suggesting that the adhesion geometry of a population of vesicles with identical composition can be broadly summarized by their average α value (Figure 2e).

The Contact Angle of Adhered Vesicles Is Linked to Their Stiffness. Liposomes in the chosen series (DOPC, POPC, DPPC, and DSPC) have increasing κ values,[41−43] which in the absence of osmotic imbalances across the membrane result in a correspondingly increasing k_S trend.

We first verified this assumption via AFM-FS experiments, measuring an increasing trend of κ in the range of 9–20 k_BT and a correspondingly increasing trend of k_S values in the 10–40 mN/m range for the POPC-DPPC-DSPC series, in accordance with previously reported values obtained with this technique.[26,40] We then compared these measurements to the image analysis results described above; Figure 2e shows a comparison of the contact angle distributions for each type of liposome. All α value distributions are roughly symmetrical around a median value, which is different for each liposome and increases along the series. As hypothesized, stiffer vesicles become less oblate than softer ones upon adhesion, and their α values are on average correspondingly larger. All distributions plotted in Figure 2e are significantly different (*t* tests, all pairs, $P \leq 0.0001$). This suggests that comparing the distribution of contact angles observed via AFM imaging enables the mechanical differentiation of vesicular samples having similar size distributions.

Data reported in Figure 2 also suggest that the chosen liposome series spans over the entire range of practically measurable α values.

DOPC is the softest liposome we could successfully deposit on the employed PLL-functionalized substrates. The size distribution of intact DOPC vesicles on the surface (Figure 2a) is significantly lower than those of the other three liposomes, while it was measured to be similar to that of the POPC sample in solution (see Figure S5), suggesting that larger DOPC vesicles were either ruptured by adhesion forces or were so compliant as to be mistaken for punctured vesicles and not included in successive analysis. Moreover, even clearly intact vesicles were extremely oblate in shape, with very low H_S values. This made it necessary to lower the height threshold used to detect features during image analysis (see materials and methods). The threshold cannot of course be lowered indefinitely due to intrinsic roughness and instrumental noise; in practice, this sets ~30° as the lowest reliably measurable α values on soft vesicular objects. At the opposite end of the range, DPPC and DSPC α distributions are substantially overlapping, even if their reported κ values are quite different.[44,45] This could be explained by the fact that very stiff vesicles, only experiencing limited deformation upon interaction with the substrate, might have an insufficient contact area to provide stable adhesion, and due to this, they might detach from the surface more readily than softer vesicles when probed by the AFM tip. We indeed observed a high proportion of detachment artifacts (vesicles suddenly "disappearing" in successive scan lines) in DSPC samples.

https://dx.doi.org/10.1021/acs.analchem.9b05716
Anal. Chem. 2020, 92, 10274−10282

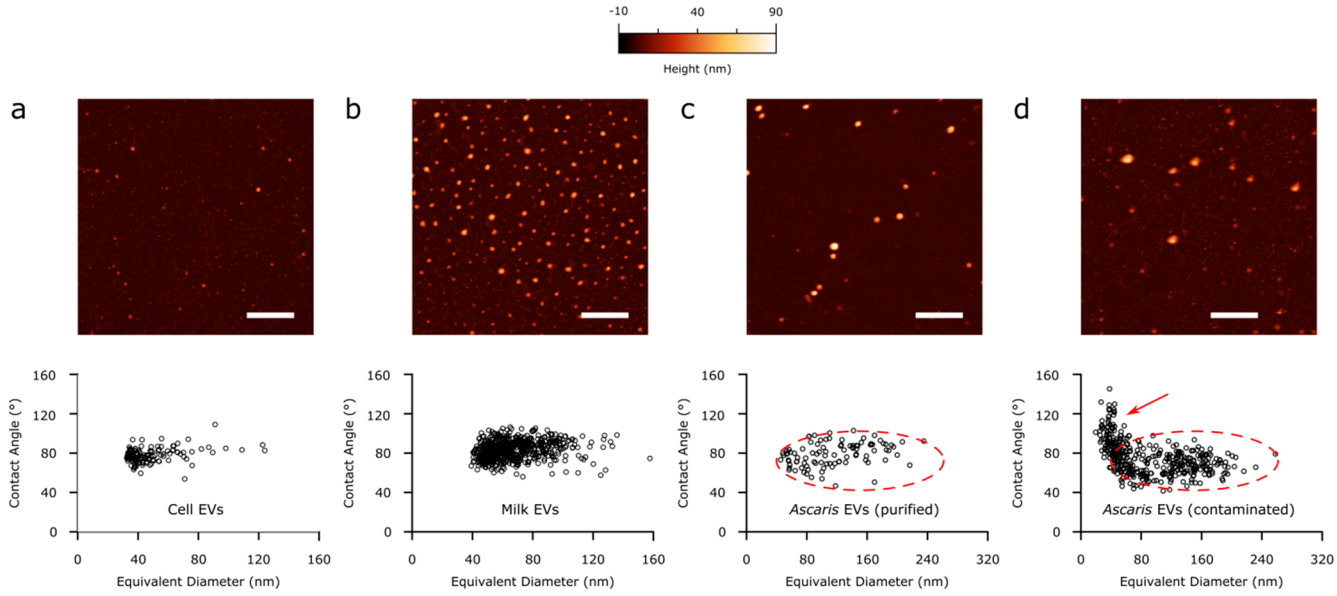

Figure 3. Representative AFM images (top row) and contact angle vs equivalent diameter scatterplots (bottom) of natural EV samples enriched from different sources. (a) EVs purified from HCT116 cell culture. (b) EVs purified from bovine milk. (c) EVs purified from *Ascaris suum* ES fractions. (d) Mycoplasma-contaminated *Ascaris suum* EVs. All purified EV samples show a relatively small dispersion of contact angles around the same average value at all sizes, resulting in horizontally elongated clusters with very weak or absent correlation between α and D_L. Nonvesicular contaminants (red arrow in panel d) do not follow this behavior and appear as an additional cluster with large contact angle variations. *Ascaris* EVs in both purified and contaminated samples appear in the same zone of the plot (panels b and c, dashed ovals).

Therefore, the α distribution of DSPC is probably biased toward lower values due to the difficulty of measuring stiffer (and weakly anchored) vesicles.

Taken together, the above considerations seem to imply that negatively charged vesicles having a stiffness between those of DOPC and DSPC should have a practically measurable α range of 30−140° when deposited on PLL-functionalized substrate and that their average α value should be a function of their k_S.

Measuring the Contact Angle of Natural EVs. The same procedure can be applied to samples containing natural vesicles. As reported by Vorselen et al.,[21] the mechanical behavior of EVs qualitatively follows that of synthetic liposomes of similar size, even in the presence of molecular cargo and integral membrane proteins. Due to this, we expect samples containing a population of EVs with small size and compositional variance to have a correspondingly small α dispersion.

We first tested the above hypothesis applying the same procedure used for liposomes on a commercially available "exosome standard" containing EVs isolated from HCT116 cell culture (see materials and methods). As expected, the resulting α versus D_L plot (Figure 3a) shows all vesicles falling in a relatively narrow range of α values regardless of their size, resulting in a horizontally elongated cluster which is indicative of vesicle-like mechanical behavior. We then repeated the analysis on natural EV samples isolated from bovine milk (Figure 3b) and from the parasitic nematode *Ascaris suum* excretory/secretory products (Figure 3c). In both cases, EVs cluster around a characteristic α value at all sizes, confirming that the purely vesicular nature of the examined samples can be mechanically assessed as previously described for liposomes.

Interestingly, the α values of all examined natural EVs seem to fall in a relatively narrow range, which corresponds to k_S values between those of POPC and DPPC liposomes: α = 83° ± 8° for HCT116 EVs, 87° ± 7° for bovine milk EVs, and 81° ± 10° for *Ascaris* EVs. This observation is compatible with the fact that different natural vesicles can show strikingly similar mechanical properties.[17] By combining typical EV size constraints (diameter ∼40−300 nm) with observed typical EV α values (60°−100°) it is thus possible to draw the boundaries of an area in α vs D_L plot (Figure 4) which could be linked to the presence of "typical" EVs in a sample.

Contact Angle Values Can Be Used to Discriminate between EVs and Impurities. Importantly, EV-enriched samples from natural sources can contain nonvesicular contaminants which could silently bias ensemble-averaged, routine characterization techniques such as, e.g., dynamic light scattering, ζ-potential, quartz crystal microbalance, flow cytometry, and Western blot. Some types of contaminants, having a markedly different morphology from EVs (e.g., membrane patches, fibrils, pili, flagella), can be discerned from EVs by appropriate microscopy techniques, including AFM. However, a purely qualitative visual inspection approach could mistakenly identify as EVs any spurious object having the expected size distribution and a generally spherical shape (e.g., nanosized crystals, protein aggregates, polymer particles).

We propose that plotting α versus D_L distributions of an EV sample can help in assessing its purity. As discussed above, the α/D_L plot of a sample only containing compositionally similar EVs will give a horizontally elongated cluster of points characterized by an average α value. Deviations from this general behavior can be thus taken as indicative of the presence of nonvesicular contaminants.

To test the above hypothesis, we applied our purely morphometric analysis on an EV sample previously recognized as contaminated. Figure 3d shows the α/size plot of a contaminated *Ascaris suum* EV sample tested with a mycoplasma kit and found positive. The resulting "L-shaped" distribution differs significantly from a corresponding *Ascaris*

https://dx.doi.org/10.1021/acs.analchem.9b05716
Anal. Chem. 2020, 92, 10274−10282

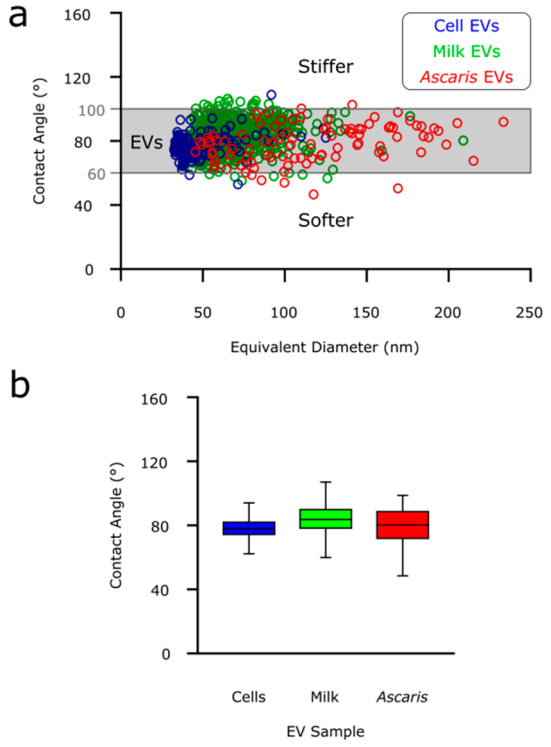

Figure 4. (a) General scheme of a contact angle vs equivalent diameter plot. The area highlighted in gray delimits values corresponding to typical mechanical behavior and size distribution of EVs deposited on a PLL substrate in ultrapure water. Individual EVs from natural sources are plotted together as blue (HCT116 cell EVs), green (milk EVs), and red (Ascaris EVs) circles. (b) Box plot comparison of EVs contact angle distributions. Boxes extend between the first (bottom edge) and third (top edge) quartile values, with black lines indicating median values. Whiskers correspond to the lowest (bottom) and highest (top) value found within the distribution. EVs from all three examined sources show a very similar stiffness.

EV sample tested negative for mycoplasma and bacteria growth (Figure 3c). Besides the expected horizontal band of points with a narrow distribution of α values (which is indicative of vesicles), an additional vertical cluster of objects with a very broad contact angle distribution is present at $D_L \sim 40$ nm. This vertical cluster of points corresponds to globular objects which were included in the morphological analysis because they could not be excluded by qualitative visual inspection alone, but which are mechanically not behaving as a single type of vesicle, thus reflecting nonvesicular contaminants in the sample. The average α value and size distributions of the horizontal clusters of Figures 3c and 3d are comparable (red dashed ovals), confirming that the two samples contain the same type of EVs. Our AFM approach can thus distinguish EVs from contaminants on the basis of their mechanical behavior and determine their respective size distributions, facilitating their characterization and successive separation.

AFM intermittent contact phase imaging or similar techniques could in principle be used to directly discriminate between globular objects with similar morphology but different physicochemical characteristics. However, we foresee that the results of these analyses would prove extremely prone to variations due to the specific AFM apparatus employed, and the results quite difficult to generalize. In our hands, the same peakforce images that allowed discriminating between EVs and contaminants using our purely morphological analysis did not provide sufficient contrast in the in-phase and quadrature channels to directly differentiate them.

Quantitative Estimation of EV Stiffness from AFM Images. To compare the results of our AFM imaging-based screening with more rigorous, FS-based nanomechanical characterization, we performed AFM-FS experiments (see Figure S1) on a series of increasingly stiffer synthetic liposomes (POPC; POPC:DPPC 1:1 mixture; DPPC; DSPC) deposited on PLL-functionalized substrates, obtaining distributions of their k_S values. We then plotted their average α versus average k_S (Figure 5), evidencing a strongly linear correlation (R^2 = 0.97). This suggests that it is possible to quantitatively estimate k_S directly from AFM imaging experiments performed on the same substrate used for a calibration line similar to Figure 5.

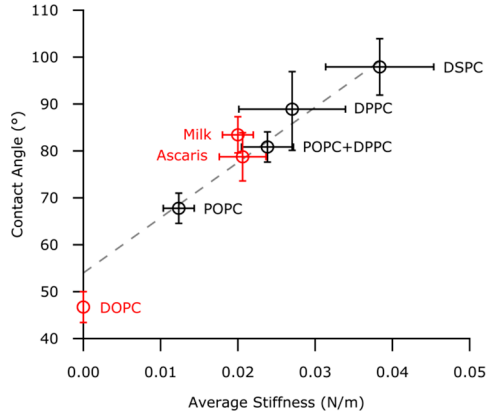

Figure 5. Quantitative correlation between average contact angle (α, measured via AFM imaging) and average stiffness (k_S, measured via AFM-FS) of vesicles deposited on PLL-functionalized glass. Black points correspond to the series of four synthetic liposomes which was used to quantify the α vs k_S dependency, showing a strong linear correlation (dashed gray line, R^2 = 0.97). Red points correspond to data not included in the linear fit (DOPC and natural EVs). All error bars represent the uncertainties obtained by bootstrapping (1000 repetitions of 5 draws, with replacement). DOPC was plotted at a k_S value of zero (see main text). The k_S of *Ascaris* and milk EVs (as measured via AFM-FS) is practically coincident with the value obtained by interpolating their average α on the liposome series fit and in both cases compatible with k_S values previously reported for other EVs from natural sources.

It is worthwhile to note that it was impossible for us to perform the full AFM-FS characterization (in terms of k_S, κ, and Π) on some of the samples. In particular, we did not observe measurable linear deformation regimes in any of the DOPC nanoindentation curves, making it impossible to measure its k_S via FS. Moreover, we could not measure F_T on *Ascaris* and milk EVs since the vast majority of retraction curves showed complex unfolding/detachment behaviors rather than clean tether elongation plateaus (see Figure S1). Nevertheless, we could easily obtain α/size plots for both samples and then estimate their expected stiffness values via extrapolation or interpolation of the linear fit shown in Figure 5.

Extrapolating the expected k_S of DOPC from its average α yields a nonphysical (negative) value. We interpreted this as a sign of a very low k_S value. Interestingly, individual approach/retraction cycles performed on intact DOPC vesicles often show clear tether elongation plateaus on the retraction curve at

https://dx.doi.org/10.1021/acs.analchem.9b05716
Anal. Chem. 2020, 92, 10274−10282

a specific F_T but no linear indentation slope on the corresponding approach curve. This suggests that the low k_S of DOPC results in very shallow indentation "slopes" which cannot be distinguished from instrumental noise. Interestingly, if we place DOPC in the α vs k_S plot (Figure 5) by assigning it a k_S value equal to 0 and then include it in the linear calibration, the correlation remains highly linear (R^2 = 0.98), further reinforcing the observation that α and k_S are strongly interdependent across a wide range of values.

We then performed the same α-based k_S extrapolation on *Ascaris* EVs, resulting in an expected stiffness value of 21 ± 4 mN/m. In this case, however, it was also possible to check extrapolation validity by directly measuring k_S via AFM-FS; the experimentally determined stiffness of 20 ± 5 mN/m coincides with the extrapolated value and is intriguingly similar to previous k_S measurements performed on other types of natural vesicles.[21,40] *Ascaris* EVs' experimental point in Figure 5, plotted at their average α (from image analysis) and k_S (from FS), is intercepted by the linear fit calculated on synthetic liposomes. The same experimental procedure was then replicated on milk EVs, obtaining strikingly similar results (k_S = 20 ± 7 mN/m, see Figure 5). Taken together, these observations suggest that the same strong correlation between α and k_S observed in liposomes is also valid for EVs and that it is thus possible to obtain a quantitative estimate of their stiffness directly from AFM image analysis, without resorting to more time-consuming FS studies. According to this reasoning, the "most typical" natural EV α value of 80° (Figure 4) corresponds to a k_S value of ∼20 mN/m.

Conclusion and Perspectives. We have herein described an AFM-based experimental strategy for the nanomechanical and morphological screening of nanosized vesicles. By the application of a set of simple experimental precautions and image analysis steps to AFM scans performed in liquid, the proposed procedure makes it possible to discriminate between vesicular and nonvesicular objects in a sample. Furthermore, it allows quantitative size and stiffness estimates for each observed vesicle. Although unable to reach the level of detail afforded by FS-based mechanical assessment methods[21,26] previously employed on EVs, the approach proposed here has the advantages of being considerably faster and easier to perform and of having limited instrumental requirements. Our results also suggest that our approach remains applicable in cases where FS-based approaches might fail.

When studied with our methodology, EVs isolated from three very different natural sources showed a similar stiffness, which is strikingly close to those previously measured on EVs from other sources.[17,21] This supports the hypothesis that the mechanical characteristics of EVs might be generally tuned for optimal diffusion velocity and deformability.[46,47] Given the wide spectrum of functions performed by EVs, ranging from cell homeostasis regulation to environmental stress-dependent signaling to extracellular matrix remodeling, the above hypothesis, if confirmed, would prove rather puzzling. We cannot of course exclude that EVs isolated from other sources might have more pronounced mechanical differences than those analyzed in our study, which would facilitate their mechanical differentiation.

Being based on the quantitative measurement of contact angles of vesicles adhered to a surface, our method could be extended to other substrates in addition to the PLL-functionalized glass slides employed in this study. This could be functional in modulating surface/vesicle adhesion forces, thus making it possible to better explore vesicles softer than DOPC or stiffer than DSPC by bringing them into the measurable α range or by extending it to the study of positively charged artificial vesicles. Its ability to quickly give a quantitative readout of the interaction between a vesicular object and a nanoengineered surface could be a valid support in developing more quantitative and more reproducible bionanomaterial research studies focusing on or involving the bionanointerface.[48]

Lastly, the geometrical parameters H_S and R_{Proj} can be also used to calculate the volume of each individual adsorbed vesicle in an AFM image. Similarly to how α is linked to k_S, any measured loss of volume induced by surface adhesion may be linked to Π; it might be thus possible to estimate lumen pressurization without resorting to complex FS experiments. We plan to explore this possibility in forthcoming studies.

In summary, we described a simple AFM-based characterization strategy that can be implemented for the nanomechanical and morphological screening of samples enriched in nanosized EVs. We showed that this method can be used to discriminate between EVs and non-EV contaminants and that it enables the high-throughput quantitative nanomechanical measurement of individual EVs, offering a simple way to implement a multiparametric characterization of EVs with nanomechanical information.

■ ASSOCIATED CONTENT

Supporting Information

The Supporting Information is available free of charge at https://pubs.acs.org/doi/10.1021/acs.analchem.9b05716.

Additional details on (i) synthetic and natural vesicles preparation, purification, and deposition; (ii) trigonometry calculations; (iii) mechanical characterization of individual vesicles by AFM force spectroscopy; (iv) AFM imaging and morphometry analysis; (v) influence of AFM probe on the nanomechanical characterization of vesicles; (vi) robustness of the image analysis procedure with respect to imaging quality; dynamic light scattering (DLS), and zeta potential characterization of liposomes; (vii) characterizations of EVs from natural sources (PDF)

■ AUTHOR INFORMATION

Corresponding Authors

Marco Brucale − *Consorzio Interuniversitario per lo Sviluppo dei Sistemi a Grande Interfase, 50019 Firenze, Italy; Consiglio Nazionale delle Ricerche, Istituto per lo Studio dei Materiali Nanostrutturati, 40129 Bologna, Italy;* orcid.org/0000-0001-7244-4389; Email: marco.brucale@cnr.it

Francesco Valle − *Consorzio Interuniversitario per lo Sviluppo dei Sistemi a Grande Interfase, 50019 Firenze, Italy; Consiglio Nazionale delle Ricerche, Istituto per lo Studio dei Materiali Nanostrutturati, 40129 Bologna, Italy;* orcid.org/0000-0001-5793-7206; Email: francesco.valle@cnr.it

Authors

Andrea Ridolfi − *Consorzio Interuniversitario per lo Sviluppo dei Sistemi a Grande Interfase, 50019 Firenze, Italy; Consiglio Nazionale delle Ricerche, Istituto per lo Studio dei Materiali Nanostrutturati, 40129 Bologna, Italy; Dipartimento di Chimica "Ugo Schiff", Università degli Studi di Firenze, 50019 Firenze, Italy*

Costanza Montis − *Consorzio Interuniversitario per lo Sviluppo dei Sistemi a Grande Interfase, 50019 Firenze, Italy; Dipartimento di Chimica "Ugo Schiff", Università degli Studi di Firenze, 50019 Firenze, Italy;* orcid.org/0000-0001-6960-3772

Lucrezia Caselli − *Dipartimento di Chimica "Ugo Schiff", Università degli Studi di Firenze, 50019 Firenze, Italy*

Lucia Paolini − *Consorzio Interuniversitario per lo Sviluppo dei Sistemi a Grande Interfase, 50019 Firenze, Italy; Dipartimento di Medicina Molecolare e Traslazionale, Università degli Studi di Brescia, 25123 Brescia, Italy;* orcid.org/0000-0002-4410-5272

Anne Borup − *Department of Clinical Medicine, Faculty of Health, Aarhus University, 8200 Aarhus, Denmark*

Anders T. Boysen − *Department of Clinical Medicine, Faculty of Health, Aarhus University, 8200 Aarhus, Denmark;* orcid.org/0000-0002-0192-1413

Francesca Loria − *HansaBiomed Life Sciences, 12618 Tallinn, Estonia*

Martijn J. C. van Herwijnen − *Department of Biochemistry & Cell Biology, Faculty of Veterinary Medicine, Utrecht University, 3584 CM Utrecht, The Netherlands*

Marije Kleinjan − *Department of Biochemistry & Cell Biology, Faculty of Veterinary Medicine, Utrecht University, 3584 CM Utrecht, The Netherlands*

Peter Nejsum − *Department of Clinical Medicine, Faculty of Health, Aarhus University, 8200 Aarhus, Denmark*

Natasa Zarovni − *HansaBiomed Life Sciences, 12618 Tallinn, Estonia*

Marca H. M. Wauben − *Department of Biochemistry & Cell Biology, Faculty of Veterinary Medicine, Utrecht University, 3584 CM Utrecht, The Netherlands*

Debora Berti − *Consorzio Interuniversitario per lo Sviluppo dei Sistemi a Grande Interfase, 50019 Firenze, Italy; Dipartimento di Chimica "Ugo Schiff", Università degli Studi di Firenze, 50019 Firenze, Italy;* orcid.org/0000-0001-8967-560X

Paolo Bergese − *Consorzio Interuniversitario per lo Sviluppo dei Sistemi a Grande Interfase, 50019 Firenze, Italy; Dipartimento di Medicina Molecolare e Traslazionale, Università degli Studi di Brescia, 25123 Brescia, Italy;* orcid.org/0000-0002-4652-2168

Complete contact information is available at: https://pubs.acs.org/10.1021/acs.analchem.9b05716

Author Contributions

The manuscript was written through contributions of all authors. All authors have given approval to the final version of the manuscript.

Notes

The authors declare no competing financial interest.

■ ACKNOWLEDGMENTS

This research has received funding from the Horizon 2020 Framework Programme under the grant FETOPEN-801367 evFOUNDRY. P.N. was supported by a grant from Independent Research Fund Denmark (DFF-6111-00521). We thank the SPM@ISMN research facility for support in the AFM experiments.

■ REFERENCES

(1) van Niel, G.; D'Angelo, G.; Raposo, G. *Nat. Rev. Mol. Cell Biol.* **2018**, *19*, 213−228.
(2) Yanez-Mo, M.; et al. *J. Extracell. Vesicles* **2015**, *4*, 27066.
(3) Galieva, L. R.; James, V.; Mukhamedshina, Y. O.; Rizvanov, A. A. *Front. Neurosci.* **2019**, *13*, 13.
(4) Mardahl, M.; Borup, A.; Nejsum, P. *Adv. Parasitol.* **2019**, *104*, 39−112.
(5) Ostenfeld, M. S.; et al. *Cancer Res.* **2014**, *74*, 5758−5771.
(6) Roy, S.; Hochberg, F. H.; Jones, P. S. *J. Extracell. Vesicles* **2018**, *7*, 1438720.
(7) van Herwijnen, M. J. C.; Driedonks, T. A. P.; Snoek, B. L.; Kroon, A. M. T.; Kleinjan, M.; Jorritsma, R.; Pieterse, C. M. J.; Hoen, E. N. M. N.; Wauben, M. H. M. *Front Nutr* **2018**, *5*, 5.
(8) Vescovi, R.; et al. *Cancer Immunol. Res.* **2019**, *7*, 12−28.
(9) Xu, R.; Rai, A.; Chen, M. S.; Suwakulsiri, W.; Greening, D. W.; Simpson, R. J. *Nat. Rev. Clin. Oncol.* **2018**, *15*, 617−638.
(10) Thery, C. *J. Extracell. Vesicles* **2018**, *7*, 1535750.
(11) Cocucci, E.; Meldolesi, J. *Trends Cell Biol.* **2015**, *25*, 364−372.
(12) Jeppesen, D. K.; Hvam, M. L.; Primdahl-Bengtson, B.; Boysen, A. T.; Whitehead, B.; Dyrskjot, L.; Orntoft, T. F.; Howard, K. A.; Ostenfeld, M. S. *J. Extracell. Vesicles* **2014**, *3*, 25011.
(13) Montis, C.; Zendrini, A.; Valle, F.; Busatto, S.; Paolini, L.; Radeghieri, A.; Salvatore, A.; Berti, D.; Bergese, P. *Colloids Surf., B* **2017**, *158*, 331−338.
(14) Shao, H. L.; Im, H.; Castro, C. M.; Breakefield, X.; Weissleder, R.; Lee, H. H. *Chem. Rev.* **2018**, *118*, 1917−1950.
(15) Paolini, L.; Zendrini, A.; Radeghieri, A. *Biomarkers Med.* **2018**, *12*, 383−391.
(16) Chiang, C. Y.; Chen, C. C. Toward characterizing extracellular vesicles at a single-particle level. *J. Biomed. Sci.* **2019**, *26*. DOI: 10.1186/s12929-019-0502-4.
(17) Sorkin, R.; Huisjes, R.; Boskovic, F.; Vorselen, D.; Pignatelli, S.; Ofir-Birin, Y.; Leal, J. K. F.; Schiller, J.; Mullick, D.; Roos, W. H.; Bosman, G.; Regev-Rudzki, N.; Schiffelers, R. M.; Wuite, G. J. L. *Small* **2018**, *14*, 1801650.
(18) Calo, A.; Reguera, D.; Oncins, G.; Persuy, M. A.; Sanz, G.; Lobasso, S.; Corcelli, A.; Pajot-Augy, E.; Gomila, G. *Nanoscale* **2014**, *6*, 2275−2285.
(19) Parisse, P.; Rago, I.; Severino, L. U.; Perissinotto, F.; Ambrosetti, E.; Paoletti, P.; Ricci, M.; Beltrami, A. P.; Cesselli, D.; Casalis, L. *Eur. Biophys. J.* **2017**, *46*, 813−820.
(20) Sharma, S.; Rasool, H. I.; Palanisamy, V.; Mathisen, C.; Schmidt, M.; Wong, D. T.; Gimzewski, J. K. *ACS Nano* **2010**, *4*, 1921−1926.
(21) Vorselen, D.; van Dommelen, S. M.; Sorkin, R.; Piontek, M. C.; Schiller, J.; Dopp, S. T.; Kooijmans, S. A. A.; van Oirschot, B. A.; Versluijs, B. A.; Bierings, M. B.; van Wijk, R.; Schiffelers, R. M.; Wuite, G. J. L.; Roos, W. H. *Nat. Commun.* **2018**, *9*, 9.
(22) Krieg, M.; Fläschner, G.; Alsteens, D.; Gaub, B. M.; Roos, W. H.; Wuite, G. J. L.; Gaub, H. E.; Gerber, C.; Dufrêne, Y. F.; Müller, D. J. *Nature Reviews Physics* **2019**, *1*, 41−57.
(23) Whitehead, B.; Wu, L.; Hvam, M. L.; Aslan, H.; Dong, M.; Dyrskjøt, L.; Ostenfeld, M. S.; Moghimi, S. M.; Howard, K. A. *J. Extracell. Vesicles* **2015**, *4*, 29685−29685.
(24) Canham, P. B. *J. Theor. Biol.* **1970**, *26*, 61−81.
(25) Helfrich, W. *Z. Naturforsch., C: J. Biosci.* **1973**, *28*, 693−703.
(26) Vorselen, D.; MacKintosh, F. C.; Roos, W. H.; Wuite, G. J. L. *ACS Nano* **2017**, *11*, 2628−2636.
(27) Valle, F.; Brucale, M.; Chiodini, S.; Bystrenova, E.; Albonetti, C. *Micron* **2017**, *100*, 60−72.
(28) Seifert, U.; Lipowsky, R. *Phys. Rev. A: At., Mol., Opt. Phys.* **1990**, *42*, 4768−4771.
(29) Jackman, J. A.; Choi, J. H.; Zhdanov, V. P.; Cho, N. J. *Langmuir* **2013**, *29*, 11375−11384.
(30) Buzas, E. I.; Toth, E. A.; Sodar, B. W.; Szabo-Taylor, K. E. *Semin. Immunopathol.* **2018**, *40*, 453−464.
(31) Deregibus, M. C.; Figliolini, F.; D'antico, S.; Manzini, P. M.; Pasquino, C.; De Lena, M.; Tetta, C.; Brizzi, M. F.; Camussi, G. *Int. J. Mol. Med.* **2016**, *38*, 1359−1366.
(32) Konoshenko, M. Y.; Lekchnov, E. A.; Vlassov, A. V.; Laktionov, P. P. *BioMed Res. Int.* **2018**, *2018*, 1.

(33) Reviakine, I.; Gallego, M.; Johannsmann, D.; Tellechea, E. *J. Chem. Phys.* **2012**, *136*, 084702.
(34) Piontek, M. C.; Lira, R. B.; Roos, W. H. *Biochim. Biophys. Acta, Gen. Subj.* **2019**, 129486.
(35) Et-Thakafy, O.; Delorme, N.; Gaillard, C.; Meriadec, C.; Artzner, F.; Lopez, C.; Guyomarc'h, F. *Langmuir* **2017**, *33*, 5117−5126.
(36) Yokota, S.; Kuramochi, H.; Okubo, K.; Iwaya, A.; Tsuchiya, S.; Ichiki, T. *PLoS One* **2019**, *14*, e0224091.
(37) Chernyshev, V. S.; Rachamadugu, R.; Tseng, Y. H.; Belnap, D. M.; Jia, Y.; Branch, K. J.; Butterfield, A. E.; Pease, L. F., 3rd; Bernard, P. S.; Skliar, M. *Anal. Bioanal. Chem.* **2015**, *407*, 3285−3301.
(38) Skliar, M.; Chernyshev, V. S.; Belnap, D. M.; Sergey, G. V.; Al-Hakami, S. M.; Bernard, P. S.; Stijleman, I. J.; Rachamadugu, R. *Biochem. Biophys. Res. Commun.* **2018**, *501*, 1055−1059.
(39) Skliar, M.; Chernyshev, V. S. *J. Visualized Exp.* **2019**, *151*, e59254.
(40) Li, S.; Eghiaian, F.; Sieben, C.; Herrmann, A.; Schaap, I. A. T. *Biophys. J.* **2011**, *100*, 637−645.
(41) Dimova, R. *Adv. Colloid Interface Sci.* **2014**, *208*, 225−234.
(42) Nagle, J. F. *Faraday Discuss.* **2013**, *161*, 11−29.
(43) Yi, Z.; Nagao, M.; Bossev, D. P. *J. Phys.: Condens. Matter* **2009**, *21*, 155104.
(44) Fernandezpuente, L.; Bivas, I.; Mitov, M. D.; Meleard, P. *Europhys. Lett.* **1994**, *28*, 181−186.
(45) Marsh, D. *Chem. Phys. Lipids* **2006**, *144*, 146−159.
(46) Dai, Z.; Yu, M. R.; Yi, X.; Wu, Z. M.; Tian, F. L.; Miao, Y. Q.; Song, W. Y.; He, S. F.; Ahmad, E.; Guo, S. Y.; Zhu, C. L.; Zhang, X. X.; Li, Y. M.; Shi, X. H.; Wang, R.; Gan, Y. *ACS Nano* **2019**, *13*, 7676−7689.
(47) Yu, M. R.; Song, W. Y.; Tian, F. L.; Dai, Z.; Zhu, Q. L.; Ahmad, E.; Guo, S. Y.; Zhu, C. L.; Zhong, H. J.; Yuan, Y. C.; Zhang, T.; Yi, X.; Shi, X. H.; Gan, Y.; Gao, H. J. *Proc. Natl. Acad. Sci. U. S. A.* **2019**, *116*, 5362−5369.
(48) Faria, M.; Bjornmalm, M.; Thurecht, K. J.; Kent, S. J.; Parton, R. G.; Kavallaris, M.; Johnston, A. P. R.; Gooding, J. J.; Corrie, S. R.; Boyd, B. J.; Thordarson, P.; Whittaker, A. K.; Stevens, M. M.; Prestidge, C. A.; Porter, C. J. H.; Parak, W. J.; Davis, T. P.; Crampin, E. J.; Caruso, F. *Nat. Nanotechnol.* **2018**, *13*, 777−785.

https://dx.doi.org/10.1021/acs.analchem.9b05716
Anal. Chem. 2020, 92, 10274−10282